Membrane-mediated interaction of intercellular cylindrical nanoparticles

Zeming Wu and Xin Yi[*]

Department of Mechanics and Engineering Science, College of Engineering, Peking University, Beijing 100871, P. R. China

Nanoparticles in intercellular gaps, junctions, or seals could have close contact with neighboring cells simultaneously. Understanding the interaction between intercellular nanoparticles and confining cell membranes is of fundamental importance, not only to the unravelling of endocytic mechanisms but also to implications such as controlled drug delivery in tumor tissues. Here we theoretically examine the mechanical behaviors of adhesive cylindrical nanoparticles confined between two lipid membrane patches of finite size. As the size of the particle-membrane contact region or wrapping degree increases, neighboring cylindrical nanoparticles become separated and the nanoparticle distance increases first and then decreases until the particles are fully trapped by adjacent membrane patches. Depending on the nanoparticle size, adhesion energy, membrane bending rigidity and tension, and intermembrane distance, three characteristic particle-membrane interaction phases are determined as no wrapping, partial trapping, and full trapping, and the corresponding interaction phase diagram is established. Further energy comparison indicates that multiple nanoparticles undergoing the two-membrane trapping process do not exhibit cooperative effects. Analytical estimations on the system energy and configurations at equilibrium are performed based on the force balance of the membranes at small deformation and match well with numerical solutions. The results shed light on the mechanical behaviors of multiple nanoparticles in cell junctions or gaps and may have implications for drug delivery in tumor tissues.

DOI: 10.1103/PhysRevE.104.034403

I. INTRODUCTION

Cellular interaction with nanoparticles has been the subject of renewed focus for decades owing to its fundamental necessity in many fields of physical and molecular biology of cells, nanomedicine, and safe applications of nanotechnology, such as endocytosis, drug delivery, and nanomaterial safety [1–3]. Once the nanoparticles come into contact with a cell, the overall adhesive force arising from either specific binding or nonspecific interaction between the nanoparticle and cell membrane, or both, lowers the free energy of interaction, and leads the membrane curving and wrapping around the nanoparticle at the cost of elastic deformation energy from membrane bending and tension as well as possible particle deformation. The free-energy reduction from the energetic competition mentioned above drives the wrapping process until the nanoparticle is fully wrapped by the cell membrane. Nanoparticles attaching on a cell surface or in a dilute cell cluster are interacting with a single cell membrane, and it has become well-known that the single-membrane wrapping around nanoparticles exhibits dependence of particle size, shape, elasticity and surface functionalization [1–4]. For example, the cell uptake of nanoparticles is regulated not only by the particle stiffness [5] but also the substrate stiffness [6]. In cases of two identical spherical nanoparticles binding to a membrane, the membrane-mediated interaction between particles on the same membrane side could be attractive or repulsive, depending on the wrapping degree [7];

while the interaction between spherical particles on the opposite membrane sides is always attractive [8]. Two-dimensional theoretical studies on the interaction between two rigid cylindrical nanoparticles on a membrane indicate repulsive (attractive) interaction for particles on the same (opposite) membrane side [8–11].

Other intriguing theoretical works on the membrane-mediated interaction between anisotropic nanoparticles attaching on the membrane [12] or inclusions such as membrane proteins embedded in the membrane [13–17] have also been performed. For nanoparticles attaching on the membrane, the membrane surface is intact as a simply connected region and the membrane-particle contact zone evolves as the membrane deforms and wraps around the nanoparticles, while in the case of membrane inclusion interaction the membrane is multiply connected and it could be adopted that the membrane-inclusion interface geometry and associated contact angles are fixed by the inclusion shape and central hydrophobic region.

In contrast to the single-membrane wrapping, nanoparticles confined between intercellular gaps, junctions, or seals could form tight contact with neighboring cell membranes simultaneously [18,19]. Understanding mechanical behaviors of confined nanoparticles and their interaction with confining membranes is of importance to deep drug delivery in tumor tissues, whose microenvironment is structurally heterogeneous and contains dense interstitial structures with separation distances as short as a few or tens of nanometers [20]. So far little work has been done in exploring the interaction between intercellular nanoparticles and confining cell membranes, particularly from a theoretical viewpoint [21,22]. A recent work
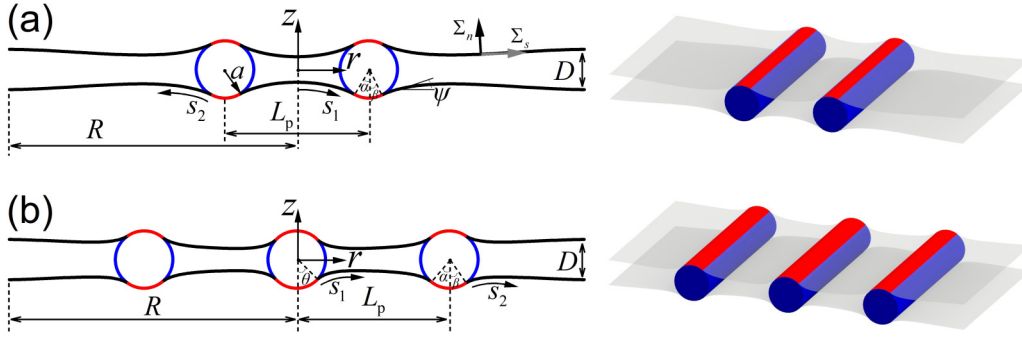
─────────
[*]xyi@pku.edu.cn

FIG. 1. Schematics of two (a) and three (b) identical parallel rigid adhesive cylindrical nanoparticles confined between two adjacent cell membranes. The vertical intermembrane distance between the membrane ends is fixed at D. A two-dimensional Cartesian coordinate rz is adopted such that these two initially flat membranes are located at $z = \pm D/2$ and the system is of mirror symmetry about the plane $r = 0$ and $z = 0$. Red curves represent regions of contact between the nanoparticles and membranes, and black and blue curves represent free parts of the membranes and particles, respectively. The distance between centers of neighboring nanoparticles is denoted by L_p. The arclength of each outer free membrane is measured from the contact edge. For the inner free membrane, its arclength is measured from the z axis in panel (a) and from the inner contact edge in panel (b).

combining experimental studies, theoretical modeling and molecular dynamics simulations demonstrates that spherical nanoparticles could be trapped in narrow intercellular seals with impeded cell uptake [21]. Further theoretical investigation reveals shape-dependent cell interaction with intercellular nanoparticles, that is, confined cylindrical nanoparticles are trapped between two neighboring membranes and confined spherical nanoparticles could undergo a state transition from two-membrane trapping to single-membrane wrapping as the wrapping degree increases [22]. It remains unclear how multiple confined nanoparticles interact with each other.

Here we perform a theoretical study on the membrane-mediated interaction of parallel infinitely long cylindrical nanoparticles confined between two adjacent lipid membranes of finite sizes. The system energy at equilibrium and corresponding trapping configurations at different values of the membrane tension and intermembrane distance are determined. The nanoparticle distance increases first and then decreases as the wrapping degree increases. It is also found that there is no visible cooperative trapping for these confined nanoparticles. The nanoparticle-membrane interaction phase diagram describing transition between states of no wrapping, partial trapping, and full trapping is established. Moreover, analytical attention is devoted to the system energy and configurations at small membrane deformation. Our work provides mechanistic insight into the mechanical behaviors of multiple intercellular nanoparticles, and may aid the development of deep drug delivery in tumor tissues.

II. MODEL AND METHODS

To investigate the mechanical interplay between multiple identical rigid cylindrical nanoparticles and two cell membranes of a fix intermembrane distance D, a theoretical model as shown in Fig. 1 is built in which the particle-membrane system configuration is assumed to be of mirror symmetry about the planes $r = 0$ and $z = 0$ in the adopted two-dimensional Cartesian coordinate rz. Here we concern the case of nanoparticle radius $a > D/2$. Due to the specific configuration symmetry, our theoretical analysis hereinafter is

focused on the right lower quarter of the system. At $a < D/2$, the cylindrical nanoparticles are assumed to interplay with a single membrane, and the corresponding membrane-mediated particle interaction is repulsive as previous theoretical analyses indicate [8–11].

In the case of two parallel cylindrical nanoparticles [Fig. 1(a)], the membrane is divided into three portions: inner free, outer free, and contact regions. Quantities pertaining to the inner and outer free membrane regions are identified by subscripts 1 and 2, respectively. Adopting the Canham-Helfrich membrane theory [23,24], the membrane elastic energy per unit length in the out-of-plane direction is [5,9,11,12]

$$E_{el} = 4 \times \left[\frac{\kappa}{2} \sum_{i=1,2} \int_0^{l_i} \left(\frac{d\psi_i}{ds_i} \right)^2 ds_i + \sigma \Delta L + \frac{\pi\kappa}{2a} f \right], \quad (1)$$

where κ and σ represent the bending rigidity and a constant lateral tension of the membrane, respectively; ψ_i, s_i, and l_i denote the tangent angle, arclength, total arclength of the free membrane region, respectively. $\Delta L = \sum_{i=1,2} \int_0^{l_i} (1 - \cos\psi_i) ds_i + a[\pi f/2 - (\sin\alpha + \sin\beta)]$ is the excess length induced by membrane wrapping, where α and β denote the contact angles between the cylindrical nanoparticle and the inner and outer free membrane regions, respectively. The wrapping degree is $f = (\alpha + \beta)/\pi$ as the length ratio between the contact region and the circumference of the cylindrical nanoparticle. Zero membrane spontaneous curvature is assumed. In Eq. (1), the assumption of the constant membrane tension σ presupposes a membrane area reservoir. The membrane tension σ, characterizing the energetic cost of pulling excess area from the reservoir, can also be understood as a chemical potential for the total membrane area in the sense of a constant area per lipid [25]. Values of the membrane tension could vary in a wide range from 0.003 mN/m to 2 mN/m [26]. For example, the membrane tension of neurons falls in a range from 0.003 mN/m to 0.04 mN/m [27]. Within the brackets in Eq. (1), the first term denotes the membrane bending energy of the free regions, the second term is the membrane tension energy, and the third term represents the membrane bending

energy of the contact region. The prefactor 4 arises from equal energy contribution from four quarters of the system.

By introducing a new variable $t_i \equiv s_i/l_i$ and converting the integral interval $[0, l_i]$ for s_i to a unit interval $[0,1]$ for t_i, Eq. (1) can be expressed as

$$\frac{E_{el}}{4\kappa/a} = \sum_{i=1,2} \frac{a}{2l_i} \int_0^1 \left(\frac{d\psi_i}{dt_i}\right)^2 dt_i + \frac{2\sigma a^2}{\kappa} \times \frac{\Delta L}{2a} + \frac{\pi}{2}f.$$

The total system energy is $E_{tot} = E_{el} - \gamma \times 4\pi af$, where $\gamma (>0)$ is the nanoparticle-membrane adhesion energy. In a dimensionless form, one has

$$\frac{E_{tot}(\bar{\sigma}, \bar{\gamma}, \psi_i, d\psi_i/dt_i, l_i/a)}{\kappa/a} = \frac{E_{el}}{\kappa/a} - 2\pi f\bar{\gamma},$$

where $\bar{\sigma} = 2\sigma a^2/\kappa$ and $\bar{\gamma} = 2\gamma a^2/\kappa$.

In the case of three nanoparticles [Fig. 1(b)], the membrane is divided into four portions: inner and outer free membrane regions, and inner and outer contact regions. Subscripts 1 and 2 are used to identify quantities associated with the inner and outer free membrane regions, respectively, unless stated otherwise. Therefore, the membrane elastic energy of the system is

$$E_{el} = 4 \times \left[\begin{array}{l} \dfrac{\kappa}{2} \sum_{i=1,2} \int_0^{l_i} \left(\dfrac{d\psi_i}{ds_i}\right)^2 ds_i \\[2mm] + \sigma \Delta L + \dfrac{\pi\kappa}{4a}f_1 + \dfrac{\pi\kappa}{2a}f_2 \end{array} \right], \quad (2)$$

or

$$\frac{E_{el}}{4\kappa/a} = \sum_{i=1,2} \frac{a}{2l_i} \int_0^1 \left(\frac{d\psi_i}{dt_i}\right)^2 dt_i$$
$$+ \frac{2\sigma a^2}{\kappa} \times \frac{\Delta L}{2a} + \frac{\pi}{4}(f_1 + 2f_2),$$

where $f_1 = 2\theta/\pi$ and $f_2 = (\alpha + \beta)/\pi$ represent the wrapping degrees of the inner and outer nanoparticles, respectively, and the wrapping-induced excess length is $\Delta L = \sum_{i=1,2} l_i \int_0^1 (1 - \cos\psi_i)dt_i + a[\pi(f_1 + 2f_2)/4 - (\sin\alpha + \sin\beta + \sin\theta)]$. The total system energy is

$$E_{tot} = E_{el} - \gamma \times 2\pi a(f_1 + 2f_2)$$

or in a dimensionless form as

$$\frac{E_{tot}(\bar{\sigma}, \bar{\gamma}, \psi_i, d\psi_i/dt_i, l_i/a)}{\kappa/a} = \frac{E_{el}}{\kappa/a} - \pi(f_1 + 2f_2)\bar{\gamma}.$$

With Eqs. (1) and (2) and geometric relations $dr_i/dt_i = l_i \cos\psi_i$ and $dz_i/dt_i = l_i \sin\psi_i$, the system energy and configurations can be characterized as functions of $\psi_i = \psi_i(t_i)$ with $t_i \in [0, 1]$ $(i = 1, 2)$. In our numerical calculations, the tangent angle ψ_i is approximated by a cubic B-spline curve $\psi_i = \sum_{j=0}^{n} c_j^{(i)} N_j^{(i)}(t_i)$, where $c_j^{(i)}$ are coefficients of the basis functions $N_j^{(i)}$ defined recursively on a knot vector of t_i. A typical choice of the knot vector of t_i in a cubic B-spline fitting is $\{t_i^{(0)}, t_i^{(1)}, t_i^{(2)}, \ldots, t_i^{(n+4)}\}$ with $t_i^{(k)} = 0$ $(k = 0, 1, 2, 3)$ and $t_i^{(k)} = 1$ $(k = n + 1, \ldots, n + 4)$.

At a given intermembrane distance D and wrapping degree f (or f_i), the minimum energy state of the system is determined using the interior-point approach in constrained nonlinear optimization. During energy minimization the following boundary and constraint conditions provide either input parameters or equality constraints for the determination of variables $c_j^{(i)}$ and l_i.

In the case of two cylindrical nanoparticles, the center of the right nanoparticle is located at $(L_p/2, 0)$ with L_p as the prescribed distance between centers of neighboring nanoparticles. The tangent angles $\psi_1 = 0$ at the mirror plane $r = 0$ $(s_1 = 0$ or $t_1 = 0)$ and $\psi_2 = 0$ at the remote boundary $s_2 = l_2$ (or $t_2 = 1$) are required to enforce the membrane flatness there. At the contact edges, the continuities of r and z coordinates and tangent angles of the membrane are required. With the relations $r_2(l_2) = r_2(0) + l_2 \int_0^1 \cos\psi_2 dt_2$ and $z_2(l_2) = z_2(0) + l_2 \int_0^1 \sin\psi_2 dt_2$, the r and z coordinates of the end of the right lower membrane is constrained at $r_2(l_2) = R$ and $z_2(l_2) = -D/2$. We take $R = 20a$ in our calculations, unless stated otherwise. The prescribed total wrapping degree f with a partition of $f = (\alpha + \beta)/\pi$ with positive α and β acts as an equality constraint. For three nanoparticles with the prescribed particle distance L_p, the boundary and constraint conditions are quite similar to the case of two particles.

III. NUMERICAL RESULTS AND DISCUSSION

A. Membrane interaction with two confined cylindrical nanoparticles

We first probe how two cylindrical nanoparticles mechanically interact with confining membranes. As an example, we perform case studies of different values of f and $\bar{\sigma}$ at $D/a = 1.4$ (Fig. 2). It is found that the two cylindrical nanoparticles are energetically favorable to stay in contact with both membranes and be trapped between them, similar to the case of one intercellular cylindrical nanoparticle at $D/a < 2$ [22]. At $f = 0$ (no-wrapping state), the energy minimum state is at $L_p = 2a$ with two nanoparticles staying in contact with each other. Similar to this phenomenon that cylindrical nanoparticles are in tight contact at the no-wrapping state with small intermembrane distance $D < 2a$, confined spherical nanoparticles at the no-wrapping state in a membrane nanotube of a diameter $D < 2a$ stay in contact [28–30]. As f increases, two neighboring nanoparticles gradually become separated and the nanoparticle distance L_p increases first and then decreases until the nanoparticles are fully trapped by the adjacent membranes with both inner and outer regions staying in touch. In the full-trapping state [marked by the symbols in Fig. 2(c)], the nanoparticles have no exposure to external environments. For a given intermembrane distance D, the maximum value of L_p decreases as $\bar{\sigma}$ increases. During the transition from the partial-trapping state to full-trapping state, the inner membranes form contact first and then outer membranes come into contact [Figs. 2(d) and 2(e)] with a further decrease in L_p [Fig. 2(c)]. In addition to numerical calculations, theoretical predictions of the energy, particle distance, and system configuration based on small deformation assumption have also been performed in the Appendix. It is shown that the small deformation assumption works very well for the profile of particle distance versus the wrapping degree f and system configuration [see dashed lines in Figs. 2(b)–2(e)].
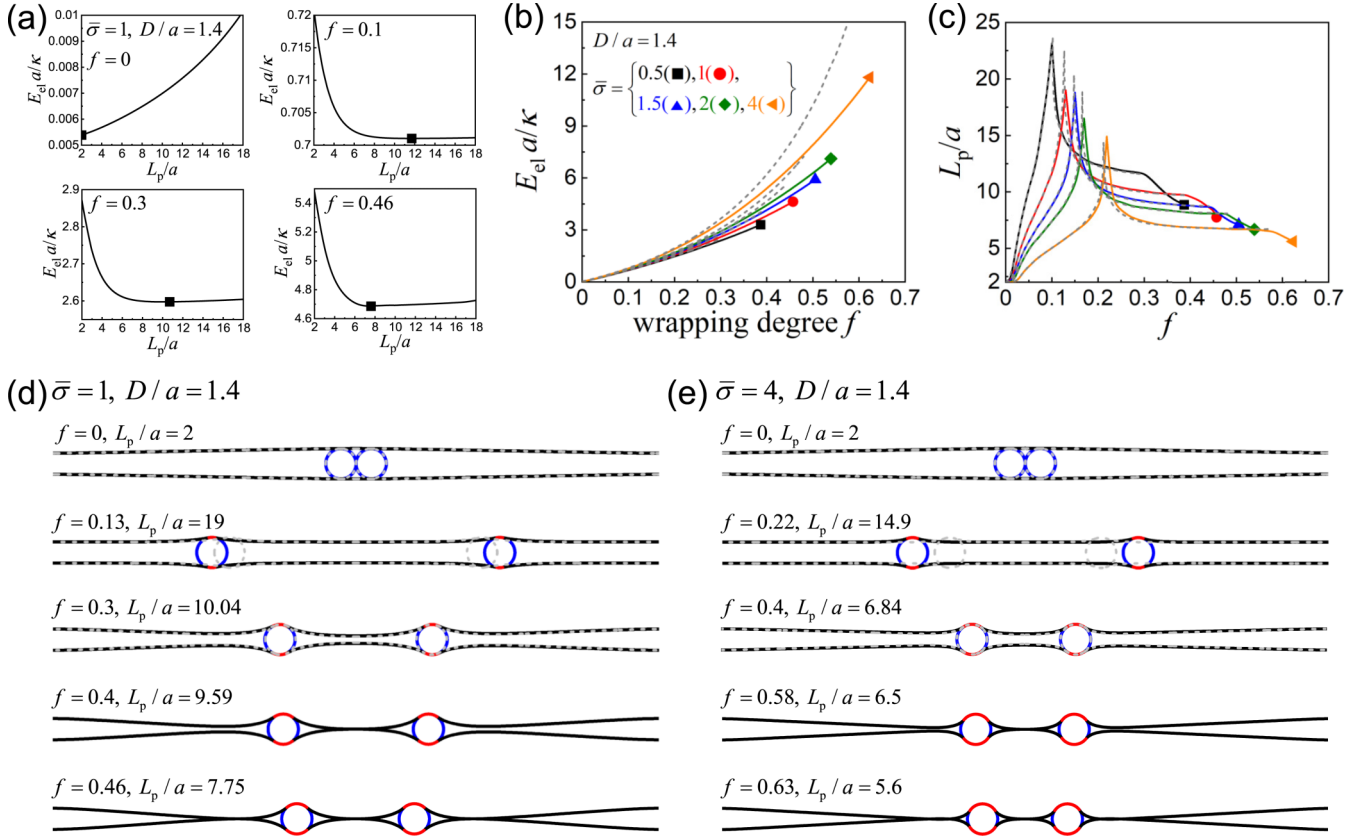
FIG. 2. Two rigid cylindrical nanoparticles interacting with confining membranes. (a) Elastic energy E_{el} as a function of the particle distance L_p for different values of the wrapping degree f at $\bar{\sigma} = 1$ and $D/a = 1.4$. (b), (c) E_{el} and L_p/a as functions of f for different $\bar{\sigma}$ at $D/a = 1.4$. (d), (e) Selected system configurations at $\bar{\sigma} = 1$ and 4. Square symbols in (a) mark the minimum energy states. Dashed lines in panels (b) and (c) represent results based on Eq. (A12), and the particle-membrane interaction states marked by symbols in panels (b) and (c) correspond to the full-trapping states with the outer membranes just in touch. Configurations in panels (d) and (e) from top to bottom correspond to five states, no-wrapping with $L_p = 2a$, partial-trapping with maximum nanoparticle distance, partial-trapping after the maximum nanoparticle distance and before inner membranes in touch, partial-trapping with inner membranes in touch, and full-trapping with both inner and outer membranes in touch. The particle-membrane interaction states marked by symbols in panels (b) and (c) correspond to the full-trapping states with the outer membranes just in touch. Dashed lines in panels (d) and (e) denote the system configuration based on small membrane deformation assumption.

Effects of the intermembrane distance D on the elastic energy profiles $E_{el}(f)$ and nanoparticle distance $L_p(f)$ at $\bar{\sigma} = 4$ are analyzed in Fig. 3. It is shown that $E_{el}(f)$ is not sensitive to D [Fig. 3(a)]. At $D/a = 2$, L_p varies mildly with f. At $D/a < 2$, there is a peak in the $L_p(f)$ profile, and the maximum nanoparticle distance L_p^{max} slightly decreases but the corresponding f significantly increases as D decreases.

Having knowledge of $E_{el}(f)$ in Figs. 2 and 3, the profile of total system energy $E_{tot} = E_{el} - \gamma \times 4\pi a f$ can be determined. Depending on the value of $\bar{\gamma}$, three interaction states can be reached (Fig. 4). At small $\bar{\gamma}$, E_{tot} increases monotonically with f and the no-wrapping state with $f = 0$ is adopted as the equilibrium state. As $\bar{\gamma}$ increases, the stable state changes from no wrapping to partial trapping. Further rise in $\bar{\gamma}$ leads to a stable state of full trapping. In the cases of partial trapping, there exist two kinds of system configurations, in one configuration there is no contact between two adjacent membranes, in the other configuration there is tight contact between the inner portions of two membranes. In

the full-trapping state, both inner and outer membranes form contact, and the particles are fully enveloped.

Based on the energy profile $E_{tot}(f)$ in Fig. 4, at equilibrium state the relationship between f and $\bar{\gamma}$ with given $\bar{\sigma}$ and D/a and further the phase diagram of the nanoparticle-membrane interaction for two confined cylindrical nanoparticles with respect to $\bar{\gamma}$ and $\bar{\sigma}$ at given D/a can be obtained and are selectively shown in Fig. 5. It is found that the minimum adhesion energy $\bar{\gamma}_{min}$ for partial trapping of two confined cylindrical nanoparticles is almost equal to 1, similar to the result for trapping of a single nanoparticle between adjacent membranes [22]. At $\bar{\gamma} < \bar{\gamma}_{min}$, $f = 0$ and two particles stay in contact. As $\bar{\gamma}$ exceeds $\bar{\gamma}_{min}$, finite f is reached and increases with increasing $\bar{\gamma}$ until the full-trapping state marked by the symbol is achieved [Fig. 5(a)]. At a given $\bar{\gamma}(> \bar{\gamma}_{min})$, the wrapping degree f increases as $\bar{\sigma}$ or D decreases. Summarizing the relationship between f and $\bar{\gamma}$, one can determine phase boundaries between the no- and partial-wrapping states as well as partial- and full-trapping states [Fig. 5(b)]. At a given D/a, $\bar{\gamma}$ required for full trapping is almost linearly
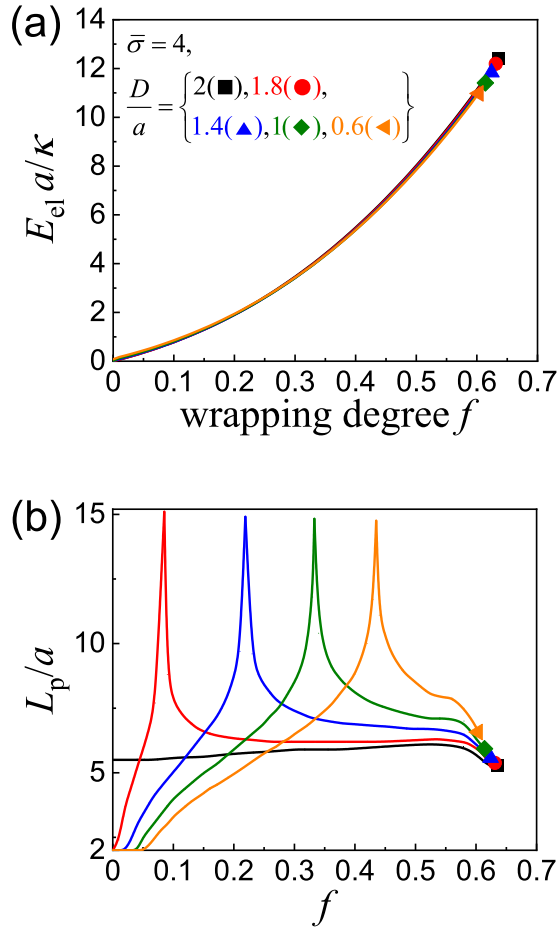
FIG. 3. Effects of the intermembrane distance D on the evolution of the elastic energy $E_{el}(f)$ and nanoparticle distance $L_p(f)$ in the case of two confined nanoparticles at $\bar{\sigma} = 4$. The particle-membrane interaction states of symbols are the full-trapping states with the outer membranes just in touch.

FIG. 4. Total energy change E_{tot} of three nanoparticle-membrane interaction states as a function of the wrapping degree f for different values of $\bar{\gamma}$ at $\bar{\sigma} = 4$ and $D/a = 1.4$. Solid symbols and the dotted red curve linking them correspond to the global minima at different $\bar{\gamma}$.

proportional to $\bar{\sigma}$. The dash-dotted lines in the partial-trapping regime denote the boundaries between the configurations with and without contact between inner membrane parts [Fig. 5(b)].

The interaction phase diagram, except the boundaries marking inner membrane touching, in Fig. 5(b) for two cylindrical nanoparticles confined between membranes is almost the same quantitatively as that for a single cylindrical nanoparticle confined between membranes (Fig. 6 in Ref. [22]). As the interaction phase diagram is a reflection of the energy profile, the above observation suggests that the presence of a second nanoparticle does not save the system elastic energy per particle and there is no visible cooperative trapping in the sense of system energy evolution. These two nanoparticles simply undergo individual trapping but in a synchronized manner of system deformation. This conclusion is also confirmed by observing that the elastic energy profiles $E_{el}(f)$ per nanoparticles is almost the same as that for the case of a single cylindrical nanoparticle confined between membranes [22].

A related phenomenon is the wrapping of multiple confined spherical nanoparticles by soft membrane nanotubes
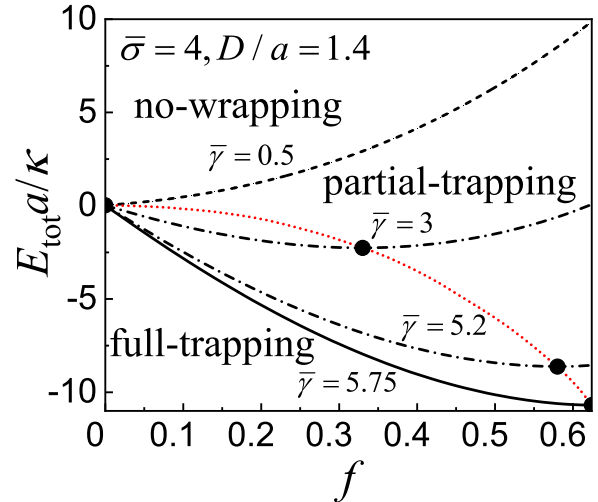
[28–30]. In the case of two identical spherical nanoparticles of radius a in a tense lipid membrane nanotube of finite length, the particle distance L_p increases from $2a$ to a maximum value and then decreases as the adhesion energy increases or equivalently the wrapping degree increases [28], similar to the trends observed in Figs. 2(c) and 3(b). In another case of packing multiple nanoparticles in a membrane nanotube with an infinite periodic pattern, it is revealed that there are two fundamental modes of interaction between these nanoparticles and the soft nanotube, the cooperative wrapping and individual wrapping [30]. At relatively small membrane tension, the cooperative wrapping is preferred [29,30]. At relatively large membrane tension, confined spherical nanoparticles at small and large wrapping degrees are cooperatively wrapped by the membrane nanotube, and particles are wrapped individually at intermediate wrapping degree [30].

In the preceding calculations, $R = 20a$ is taken and it is shown that there is a finite maximum value of L_p/a as f varies. Recalling that the membrane-mediated interaction of two cylindrical nanoparticles of circular [8–11] or elliptical [12] cross-sections attaching on the same side of an infinitely large membrane is always repulsive, one might wonder whether two cylindrical nanoparticles confined between adjacent membranes would always repel each other at an infinity R/a. To understand the effects of the membrane size on the nanoparticle-membrane interaction and indirect particle-particle interaction, profiles of elastic energy $E_{el}(f)$ and nanoparticle distance $L_p(f)$ are investigated at different values of R/a (Fig. 6). As a larger membrane leads to easier and larger deformation, the upper and lower membranes of larger size come into contact at smaller f in the full-trapping state [Fig. 6(a)]. In comparison with $E_{el}(f)$ in Fig. 6(a) showing insensitivity to R/a, the membrane size has stronger effect on $L_p(f)$. As R/a increases, the distance between the nanoparticles at equilibrium increases. One could anticipate
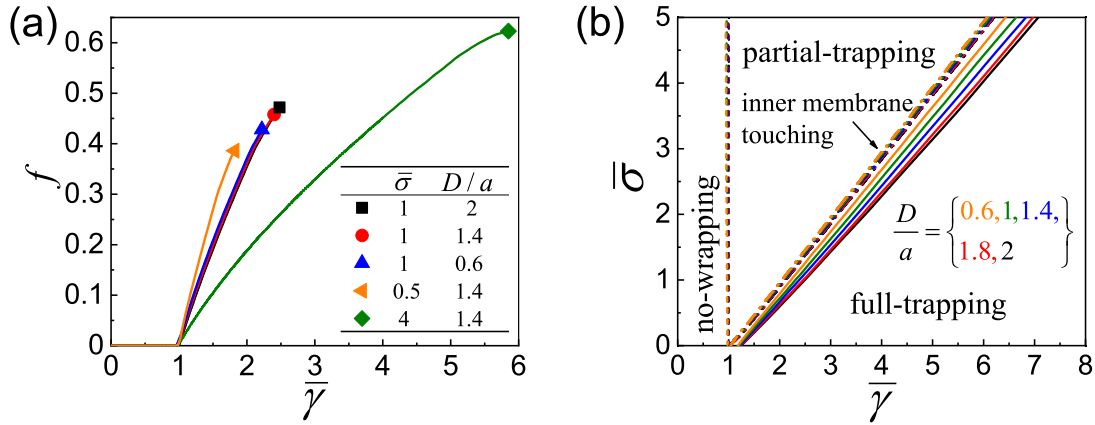
FIG. 5. (a) Wrapping degree f as a function of $\bar{\gamma}$ at different values of $\bar{\sigma}$ and D. (b) Nanoparticle-membrane interaction phase diagram with respect to $\bar{\gamma}$ and $\bar{\sigma}$ for two cylindrical particles confined between membranes at $D/a = 0.6, 1, 1.4, 1.8,$ and 2. Symbols in panel (a) mark the full-trapping states.

that L_p/a would approach infinity as the membranes become infinitely large, that is, the membrane-mediated interaction of two confined cylindrical nanoparticles between two infinity membranes at $D/a < 2$ is always repulsive.

B. Membrane interaction with three confined cylindrical nanoparticles

To gain more insight into the mechanical interplay between cylindrical nanoparticles and adjacent membranes, we now perform case studies of three confined cylindrical nanoparticles. As $\bar{\gamma}$ increases, both the wrapping degrees of the inner (f_1) and outer (f_2) particles increase; as $\bar{\sigma}$ increases, the maximum values of f_1 and f_2 increase [Fig. 7(a)]. Moreover, f_1 reaches its maximum first, that is, the inner nanoparticle reaches the full-trapping state first, as demonstrated in Fig. 7(c). Similar to the case of two confined cylindrical particles, at the no-wrapping state the nanoparticles stay in contact with each other ($L_p = 2a$). As f increases, neighboring nanoparticles become separated and L_p increases first and then decreases until all nanoparticles are fully trapped [Figs. 7(b) and 7(c)]. At a given D, the maximum value of L_p decreases as $\bar{\sigma}$ increases. Comparing Fig. 7(b) (symbols therein) and Fig. 5, one can see that more adhesion energy is

required for all three nanoparticles reaching the full-trapping state in comparison with the two-nanoparticle case. Confined cylindrical nanoparticles undergo individual trapping rather than cooperative trapping.

IV. FURTHER REMARKS

Our theoretical results indicate that the mode of interaction between confined cylindrical nanoparticles and adjacent membranes is two-membrane trapping. Adoption of the two-membrane trapping mode suggests that intercellular cylindrical nanocarriers of anticancer drugs can undergo therapeutic diffusion laterally within the membrane confinement. Our recent theoretical studies indicate that intercellular spherical nanoparticles at large adhesion energy and intermembrane distance could detach from one membrane and be wrapped by the other membrane [22]. Therefore, intercellular cylindrical nanoparticles might have a better chance of spreading throughout solid tumors rather than being engulfed nearby the tumor surface.

In the present model, the cylindrical nanoparticles are assumed to be parallel. Though this parallel alignment is only one limiting case of general mutual particle orientations, this specific orientation assumption is consistent
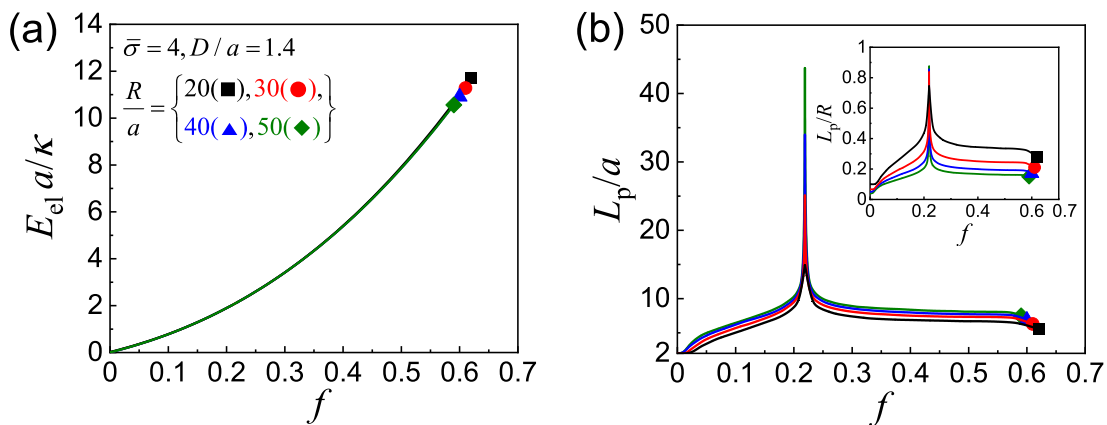

FIG. 6. Profiles of elastic energy $E_{el}(f)$ (a) and nanoparticle distance $L_p(f)$ (b) for $\bar{\sigma} = 4$ and $D/a = 1.4$ at different values of the membrane size R. Insert in panel (b) shows profiles of $L_p(f)/R$.
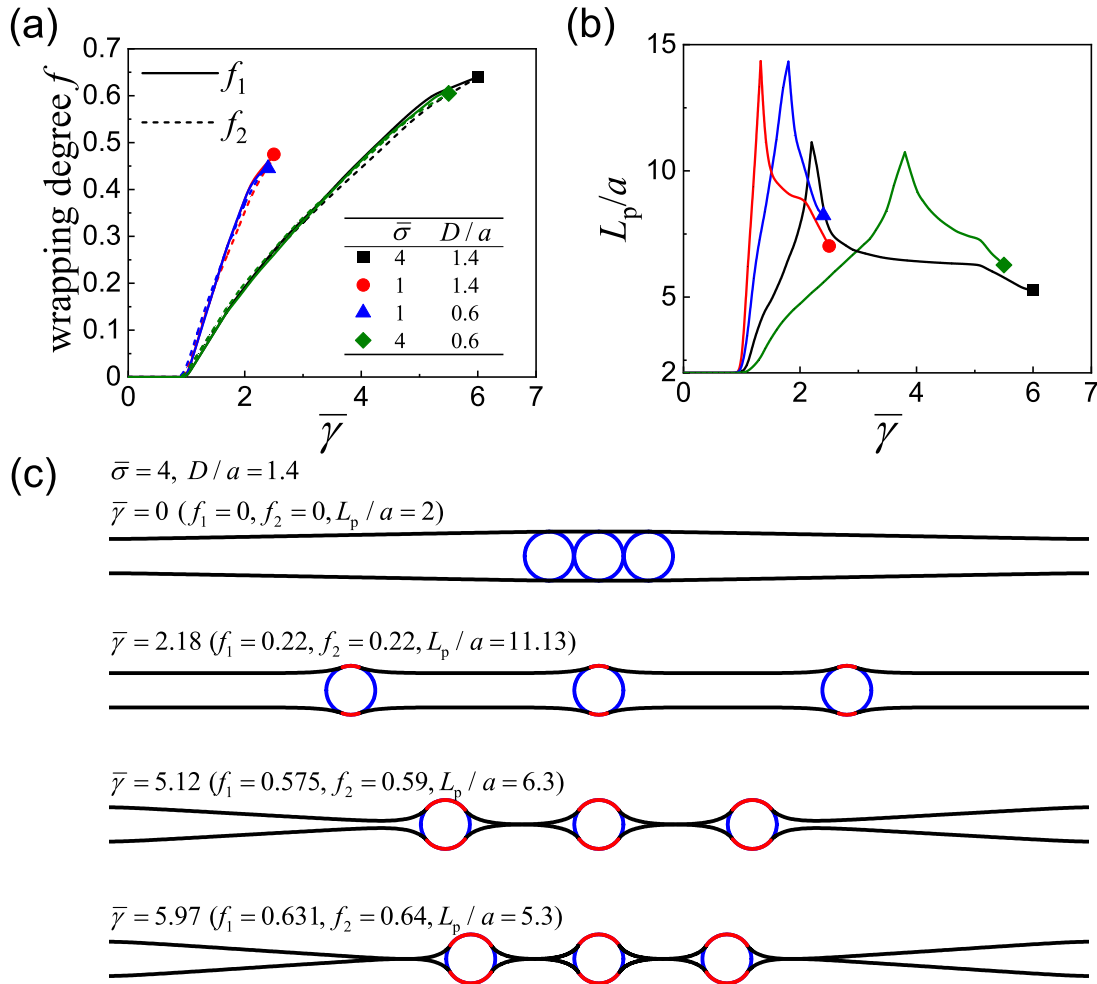
FIG. 7. Membrane interaction with three confined rigid cylindrical nanoparticles at $R/a = 20$. The wrapping degrees for inner (f_1) and outer (f_2) nanoparticles (a) and nanoparticle distance L_p (b) as functions of adhesion energy $\bar{\gamma}$ at different values of $\bar{\sigma}$ and D/a. (c) Selected system configurations for $\bar{\sigma} = 1$ and $D/a = 1.4$ at different values of $\bar{\gamma}$. Configurations in panel (c) from top to bottom correspond to the state of no wrapping with $L_p = 2a$, partial-trapping state with maximum L_p, partial-trapping state with inner membranes in touch, and full-trapping with both inner and outer membranes in touch, respectively. Symbols in panels (a) and (b) refer to the full-trapping states with the outer membranes just in touch.

with a recent theoretical study of membrane-mediated inclusion interaction which shows that two strongly elongated anisotropic membrane inclusions prefer a parallel mutual orientation via free-energy analysis [17]. A thorough and firm study on the veiled orientational distribution of confined nanoparticles with minimal assumptions is challenging and further detailed investigations are being called for.

The particle interaction mediated by the deformed membranes depends on the membrane size and wrapping degree. For infinitely large adjacent membranes at $D/a < 2$, the confined nanoparticles always repel each other. A similar repulsive membrane-mediated interaction between two cylindrical particles attaching on the same side of a single membrane holds [8–12]. For adjacent membrane patches of finite size, the distance between confined nanoparticles increases and then decreases as the wrapping degree increases, that is, there exists a maximum particle distance for finite-size membranes. The finite value of the particle distance at

the full-trapping state implies that the intercellular cylindrical nanoparticles could be distributed throughout the tumor.

A circumstance related to cylindrical nanoparticle interaction is the membrane-mediated interaction between spherical nanoparticles either attaching on the membrane [7,8] or confined between adjacent membranes [21]. For the former case, theoretical studies and molecular dynamics simulations indicate that the interaction between two spherical nanoparticles adhering to the same membrane side can be attractive or repulsive depending on the extent of membrane deformation which is regulated by the membrane bending and stretching as well as nanoparticle binding strength [7,8]. For the case of multiple intercellular spherical nanoparticles, molecular dynamics simulations demonstrate particle aggregation and so far no devoted theoretical studies have been performed. Whether the interaction is always attractive for confined spherical particles is not answered, let alone confined ellipsoidal or irregular nanoparticles. A minimal system for the confinement of nanoparticles between lipid membranes is the particle-loaded

multilayered vesicles or capsosomes with liposomal subcompartments. Understanding the interaction between membranes and confined nanoparticles is fundamentally beneficial to the development of therapeutic drug carriers.

V. CONCLUSIONS

Adopting the Canham-Helfrich membrane theory, a theoretical analysis has been performed on the membrane-mediated mechanical interaction of parallel cylindrical nanoparticles confined between two adjacent lipid membranes. The cylindrical nanoparticles are trapped therein and have contact with both membranes. The system energy at equilibrium and corresponding trapping configurations are determined using the interior-point method for constrained optimization. As the wrapping degree increases, neighboring cylindrical nanoparticles gradually become separated and the nanoparticle distance increases first and then decreases until the nanoparticles are fully trapped by adjacent membrane patches of finite size. Comparing the energy profiles per nanoparticle in the cases of single and multiple confined cylindrical nanoparticles, it is found that there is no visible cooperative trapping for multiple cylindrical nanoparticles, different from the possible cooperative wrapping of spherical nanoparticles in a membrane nanotube. The nanoparticle-membrane interaction phase diagram describing transition between states of no wrapping, partial trapping, and full trapping is determined at different intermembrane distances. It is shown that the normalized adhesion energy required for full trapping is almost linearly proportional to the normalized membrane tension. Moreover, analytical predictions on the system energy and configurations based on the force balance of the membranes at small deformation are obtained and agree well with numerical solutions. Our results provide mechanistic insight into the mechanical behaviors of multiple cylindrical nanoparticles in cell junctions or gaps, and may serve as design guidelines for rational drug delivery in tumor tissues.

APPENDIX: ANALYTICAL SOLUTIONS AT SMALL MEMBRANE DEFORMATION

In this Appendix, we analytically investigate the particle-membrane interaction based on force balance of the deformed membranes. Taking the lower membrane as example, the subscripts 1 and 2 are ignored unless they are necessary.

At zero spontaneous curvature, the local membrane force per unit length can be given as [10,31]

$$\Sigma_s = \sigma - \frac{\kappa}{2}c^2 = \sigma - \frac{\kappa}{2}\left(\frac{d\psi}{ds}\right)^2,$$

$$\Sigma_n = -\kappa\frac{dc}{ds} = -\kappa\frac{d^2\psi}{ds^2}, \qquad (A1)$$

where $c = d\psi/ds$ is the curvature of the deformed membrane, Σ_s denotes the in-plane membrane force along the arclength, and Σ_n is the out-of-plane shear force along with the normal direction.

Equations of the force balance along the vertical and horizontal directions read $\Sigma_s \sin\psi + \Sigma_n \cos\psi = F_z$ and $\Sigma_s \cos\psi - \Sigma_n \sin\psi = F_r$, respectively, with F_z and F_r as components of force on the particle along the z axis and r axis by the deformed membrane of concern. With Eqs. (A1) one has

$$\frac{F_z(s)}{\kappa} = \frac{\sigma}{\kappa}\sin\psi - \frac{1}{2}\left(\frac{d\psi}{ds}\right)^2\sin\psi - \frac{d^2\psi}{ds^2}\cos\psi, \quad (A2)$$

$$\frac{F_r(s)}{\kappa} = \frac{\sigma}{\kappa}\cos\psi - \frac{1}{2}\left(\frac{d\psi}{ds}\right)^2\cos\psi + \frac{d^2\psi}{ds^2}\sin\psi. \quad (A3)$$

Since the outer free membrane cannot freely adjust its configuration vertically with its fixed remote end, one has $F_z \neq 0$ for the outer free membrane. In contrast, for the inner membrane, one has $F_z = 0$ before the upper and lower inner membranes form contact, and the corresponding membrane configuration is exactly depicted by [10]

$$\psi_1(s_1) = -\pi - 2\mathrm{am}\left[s_1\sqrt{\frac{F_r}{\kappa m}} - K(m), m\right], \qquad (A4)$$

where $m = 2F_r/(F_r + \sigma)$, $\mathrm{am}(s, m)$ is the Jacobi amplitude with parameter m, and $K(m)$ is the complete elliptic integral of the first kind.

At small membrane deformation, one has

$$\sin\psi \approx \frac{dz}{dr}, \ \cos\psi \approx 1, \quad \frac{d\psi}{ds} \approx \frac{d^2z}{dr^2}, \frac{d^2\psi}{ds^2} \approx \frac{d^3z}{dr^3}. \quad (A5)$$

With Eq. (A5), Eqs. (A2) and (A3) become

$$\frac{d^3z}{dr^3} - \frac{\sigma}{\kappa}\frac{dz}{dr} + \frac{F_z}{\kappa} = 0, \qquad (A6)$$

$$\frac{d^3z}{dr^3}\frac{dz}{dr} - \frac{1}{2}\left(\frac{d^2z}{dr^2}\right)^2 + \frac{\sigma - F_r}{\kappa} = 0. \qquad (A7)$$

The general solution of Eq. (A6) is

$$\frac{dz}{dr} = B_1 e^{r\sqrt{\sigma/\kappa}} + B_2 e^{-r\sqrt{\sigma/\kappa}} + \frac{F_z}{\sigma},$$

where B_1, B_2, and F_z could be determined from the following boundary conditions.

For the outer free membrane, $dz_2/dr_2 = \tan\beta$ at the contact edge $s_2 = 0$ ($r_2(0) = L_\mathrm{p}/2 + a\sin\beta$), and $dz_2/dr_2 = 0$ and $\int_{r_2(0)}^{R}(dz/dr)dr = D/2 - a(1 - \cos\beta)$ at the remote end $r = R$.

Introducing $\omega = \sqrt{\sigma/\kappa}$, the above boundary conditions lead to

$$B_1 = [(e^{\omega R} - e^{\omega r_2(0)})\Omega_1 + e^{\omega r_2(0)}\Omega_3]/\Omega_4,$$

$$B_2 = -e^{\omega[r_2(0)+R]}[(e^{\omega R} - e^{\omega r_2(0)})\Omega_2 + e^{\omega R}\Omega_3]/\Omega_4,$$

$$F_z = -\sigma[e^{\omega R}\Omega_1 - e^{\omega r_2(0)}\Omega_2][e^{\omega R} - e^{\omega r_2(0)}]/\Omega_4,$$

where

$$\Omega_1 = -H\omega + \tan\beta, \quad \Omega_2 = H\omega + \tan\beta,$$
$$\Omega_3 = -\omega[R - r_2(0)]\tan\beta,$$
$$\Omega_4 = -2[e^{\omega R} - e^{\omega r_2(0)}]^2 + \omega[e^{2\omega R} - e^{2\omega r_2(0)}][R - r_2(0)],$$
$$H = D/2 - a(1 - \cos\beta).$$

Here H is introduced as the height of the outer free membrane part.

The shape of the outer free membrane is then determined as

$$z_2 = z_2(0) + \frac{F_z}{\sigma}[r_2 - r_2(0)] + \frac{B_1}{\omega}[e^{\omega r_2} - e^{\omega r_2(0)}]$$
$$+ \frac{B_2}{\omega}[e^{-\omega r_2(0)} - e^{-\omega r_2}], \tag{A8}$$

where $z_2(0) = -a\cos\beta$ is the z coordinate of the outer membrane at the contact edge.

For the inner free membrane of $F_z = 0$, from Eq. (A6) we have a general solution as

$$\frac{dz_1}{dr_1} = C_1 e^{\omega r_1} + C_2 e^{-\omega r_1}. \tag{A9}$$

From boundary conditions $dz_1/dr_1 = -\tan\alpha$ at $r_1 = r_1(s_1 = l_1) = L_p/2 - a\sin\alpha$ and $dz_1/dr_1 = 0$ at $r_1 = r_1(0) = 0$, C_1, and C_2 in Eq. (A9) are determined as

$$C_1 = -C_2 = -\frac{1}{2}\tan\alpha\, \text{csch}[\omega r_1(l_1)],$$

and the inner membrane shape is

$$z_1 = z_1(0) + \frac{\tan\alpha}{\omega}[1 - \cosh(\omega r_1)]\,\text{csch}[\omega r_1(l_1)], \tag{A10}$$

with $z_1(0) = \omega^{-1}\tan\alpha\tanh[\omega r_1(l_1)/2] - a\cos\alpha$ as the z coordinate of the inner membrane at $s_1 = 0$.

Substituting Eqs. (A8) and (A10) into Eq. (A7), the balance of horizontal forces F_r at $r_1 = 0$ and $r_2 = R$ requires

$$\left(\frac{d^2z_1}{dr_1^2}\right)^2\bigg|_{r_1=0} = \left(\frac{d^2z_2}{dr_2^2}\right)^2\bigg|_{r_2=R}. \tag{A11}$$

At given particle distance L_p and wrapping degree $f = (\alpha + \beta)/\pi$, contact angles α and β can be determined from Eq. (A11) numerically.

The particle distance L_p at a given f is determined by minimizing the total elastic energy E_{el}. The elastic energy of the membrane parts in contact regions is

$$E_c = 4 \times \left[\frac{\pi\kappa}{2a}f + \sigma a(\pi f - \sin\alpha - \sin\beta)\right].$$

For the right lower outer free membrane, the bending energy is

$$E_{bend}^{(2)} = \frac{\kappa}{2}\int_0^{l_2}\left(\frac{d\psi_2}{ds_2}\right)^2 ds_2 \approx \frac{\kappa}{2}\int_{r_2(0)}^{R}\left(\frac{d^2z_2}{dr_2^2}\right)^2 dr_2,$$

and the tension energy is

$$E_{ten}^{(2)} = \sigma\int_0^{l_2}(1 - \cos\psi_2)ds_2 \approx \frac{\sigma}{2}\int_{r_2(0)}^{R}\left(\frac{dz_2}{dr_2}\right)^2 dr_2,$$

where $\cos\psi \approx 1 - (dz/dr)^2/2$ is used.

Then we have

$$E_{bend}^{(2)} = \frac{\kappa\omega(A_1 + A_2)}{4}, \quad E_{ten}^{(2)} = \frac{A_3 + 2\sigma^2(A_1 - A_2)}{8\omega\sigma},$$

where

$$A_1 = [e^{-2\omega r_2(0)} - e^{-2\omega R}](B_1^2 e^{2I_1} + B_2^2), \quad A_2 = 4B_1 B_2 I_2,$$
$$A_3 = -4F_z^2 I_2 + 8\sigma F_z[e^{-\omega r_2(0)} - e^{-\omega R}](B_2 + B_1 e^{I_1}),$$
$$I_1 = \omega[r_2(0) + R], \quad I_2 = \omega[r_2(0) - R].$$

The energy of the outer membrane is $E_{outer} = 4 \times (E_{bend}^{(2)} + E_{ten}^{(2)})$.

Similarly, the bending and tension energy of the right lower inner free membrane are

$$E_{bend}^{(1)} = \frac{\kappa}{2}\int_0^{r_1(l_1)}\left(\frac{d^2z_1}{dr_1^2}\right)^2 dr_1$$

and

$$E_{ten}^{(1)} = \frac{\sigma}{2}\int_0^{r_1(l_1)}\left(\frac{dz_1}{dr_1}\right)^2 dr_1,$$

respectively. Then we have

$$E_{bend}^{(1)} = \frac{\kappa\omega\tan^2\alpha\,\text{csch}^2[\omega r_1(l_1)]}{8}\left\{\begin{array}{l}2\omega r_1(l_1)\\ + \sinh[2\omega r_1(l_1)]\end{array}\right\},$$

$$E_{ten}^{(1)} = \frac{\sigma\tan^2\alpha}{4\omega}\{\coth[\omega r_1(l_1)] - \omega r_1(l_1)\text{csch}^2[\omega r_1(l_1)]\},$$

and the elastic energy of the inner membrane is $E_{inner} = 4 \times (E_{bend}^{(1)} + E_{ten}^{(1)})$.

The total elastic energy at given L_p and f is

$$E_{el}(L_p, f) = E_c + E_{outer} + E_{inner},$$

and the system at given f in equilibrium and corresponding L_p are then determined by locating

$$E_{el}(f) = \min\{E_{el}(L_p, f)\} \text{ with } L_p \in [2a, 2(R - a)]. \tag{A12}$$

Comparison between theoretical results and numerical solutions and in Figs. 2(b)–2(e) shows that the small deformation assumption works very well for the profile of L_p-f and system configuration.

[1] I. Canton and G. Battaglia, Endocytosis at the nanoscale, Chem. Soc. Rev. **41**, 2718 (2012).

[2] Y. Hui, X. Yi, F. Hou, D. Wibowo, F. Zhang, D. Zhao, H. Gao, and C.-X. Zhao, Role of nanoparticle mechanical properties in cancer drug delivery, ACS Nano **13**, 7410 (2019).

[3] A. E. Nel, L. Mädler, D. Velegol, T. Xia, E. M. V. Hoek, P. Somasundaran, F. Klaessig, V. Castranova, and M. Thompson,

Understanding biophysicochemical interactions at the nano–bio interface, Nat. Mater. **8**, 543 (2009).

[4] S. Zhang, H. Gao, and G. Bao, Physical principles of nanoparticle cellular endocytosis, ACS Nano **9**, 8655 (2015).

[5] X. Yi and H. Gao, Phase diagrams and morphological evolution in wrapping of rod-shaped elastic nanoparticles by cell membrane: A two-dimensional study, Phys. Rev. E **89**, 062712 (2014).

[6] C. Huang, P. J. Butler, S. Tong, H. S. Muddana, G. Bao, and S. Zhang, Substrate stiffness regulates cellular uptake of nanoparticles, Nano Lett. **13**, 1611 (2013).

[7] B. J. Reynwar and M. Deserno, Membrane-mediated interactions between circular particles in the strongly curved regime, Soft Matter **7**, 8567 (2011).

[8] Z. Yan, Z. Wu, S. Li, X. Zhang, X. Yi, and T. Yue, Curvature-mediated cooperative wrapping of multiple nanoparticles at the same and opposite membrane sides, Nanoscale **11**, 19751 (2019).

[9] T. R. Weikl, Indirect interactions of membrane-adsorbed cylinders, Eur. Phys. J. E **12**, 265 (2003).

[10] M. M. Müller, M. Deserno, and J. Guven, Balancing torques in membrane-mediated interactions: Exact results and numerical illustrations, Phys. Rev. E **76**, 011921 (2007).

[11] S. Mkrtchyan, C. Ing, and J. Z. Y. Chen, Adhesion of cylindrical colloids to the surface of a membrane, Phys. Rev. E **81**, 011904 (2010).

[12] H. Tang, H. Ye, H. Zhang, and Y. Zheng, Wrapping of nanoparticles by the cell membrane: The role of interactions between the nanoparticles, Soft Matter **11**, 8674 (2015).

[13] T. Weikl, M. Kozlov, and W. Helfrich, Interaction of conical membrane inclusions: Effect of lateral tension, Phys. Rev. E **57**, 6988 (1998).

[14] J.-B. Fournier, Microscopic membrane elasticity and interactions among membrane inclusions: Interplay between the shape, dilation, tilt and tilt-difference modes, Eur. Phys. J. B **11**, 261 (1999).

[15] P. G. Dommersnes and J.-B. Fournier, N-body study of anisotropic membrane inclusions: Membrane-mediated interactions and ordered aggregation, Eur. Phys. J. B **12**, 9 (1999).

[16] V. I. Marchenko and C. Misbah, Elastic interaction of point defects on biological membranes, Eur. Phys. J. E **8**, 477 (2002).

[17] Y. Schweitzer and M. M. Kozlov, Membrane-mediated interaction between strongly anisotropic protein scaffolds, PLoS Comput. Biol. **11**, e1004054 (2015).

[18] H. Cabral *et al.*, Accumulation of sub-100 nm polymeric micelles in poorly permeable tumours depends on size, Nat. Nanotechnol. **6**, 815 (2011).

[19] M. M. Falk, C. L. Bell, R. M. Kells Andrews, and S. A. Murray, Molecular mechanisms regulating formation, trafficking and processing of annular gap junctions, BMC Cell Biol. **17**, S22 (2016).

[20] J. Iwasa and W. Marshall, *Karp's Cell and Molecular Biology*, 9th ed. (Wiley, Hoboken, NJ, 2020).

[21] T. Yue, H. Zhou, H. Sun, S. Li, X. Zhang, D. Cao, X. Yi, and B. Yan, Why are nanoparticles trapped at cell junctions when the cell density is high? Nanoscale **11**, 6602 (2019).

[22] Z. Wu and X. Yi, Mechanics of cell interaction with intercellular nanoparticles: Shape-dependent competition between two-membrane trapping and single-membrane wrapping, Extreme Mech. Lett. **46**, 101296 (2021).

[23] P. B. Canham, The minimum energy of bending as a possible explanation of the biconcave shape of the human red blood cell, J. Theor. Biol. **26**, 61 (1970).

[24] W. Helfrich, Elastic properties of lipid bilayers: Theory and possible experiments, Z. Naturforsch. C **28**, 693 (1973).

[25] M. Deserno, Fluid lipid membranes: From differential geometry to curvature stresses, Chem. Phys. Lipids **185**, 11 (2015).

[26] C. E. Morris and U. Homann, Cell surface area regulation and membrane tension, J. Membr. Biol. **179**, 79 (2001).

[27] J. Dai, M. P. Sheetz, X. Wan, and C. E. Morris, Membrane tension in swelling and shrinking molluscan neurons, J. Neurosci. **18**, 6681 (1998).

[28] J. Z. Y. Chen, Y. Liu, and H.-J. Liang, Structure of a Tubular Membrane Confining Spherical Particles, Phys. Rev. Lett. **102**, 168103 (2009).

[29] M. Raatz, R. Lipowsky, and T. R. Weikl, Cooperative wrapping of nanoparticles by membrane tubes, Soft Matter **10**, 3570 (2014).

[30] Z. Wu and X. Yi, Structures and mechanical behaviors of soft nanotubes confining adhesive single or multiple elastic nanoparticles, J. Mech. Phys. Solids **137**, 103867 (2020).

[31] J.-B. Fournier, On the stress and torque tensors in fluid membranes, Soft Matter **3**, 883 (2007).

Correction: The previously published Figure 5(a) was a duplicate of Figure 6(a) and has been replaced.